Complexity from Simplicity: Confinement Directs Morphogenesis

and Motility in Nematic Polymers

Arul Clement^a, Mahnoush Babaei^b, Jayanta Phadikar^a, Da Wei Lee^a, Amir Alipour Skandani^a and M. Ravi Shankar^a, *

^a Department of Industrial Engineering University of Pittsburgh, Pittsburgh PA 15261

^b Department of Mechanical Engineering Carnegie Mellon University, Pittsburgh, PA 15213

Abstract

Liquid crystalline polymers (LCP) that actuate under confinement adopt shapes with complexity that is upconverted beyond that encoded by their nascent patterning. Twisted nematic LCP thermally transform into simple spiral structures, when unconstrained. Confining them into rings or rigidly fixtured rectangular elasticas induces their self-assembly into supercoils, prismatic folded trusses, twisted and bent tape spring geometries. No additional material patterning, localized stimulation or training is required. Along its way, the actuation unlocks mechanical instabilities that can power impulsive responses. The self-assembled structures also sustain dynamic responses. These include motility via crawling and kinematic manipulation in a crank-rocker mechanism from an otherwise unstructured thermal stimulus. Interacting assemblages of the individually confined LCP build functionally relevant structures, including airframes and gripper-arm mimicking geometries. Thus, confinement is shown to free shape selection from a one-to-one correspondence to the blueprinted microstructure in active polymers.

^{*} ravishm@pitt.edu

1. Introduction

Programming morphogenesis in responsive materials has been an organizing principle behind the pursuit of self-assembly in mechanical systems. The natural world often inspires these pursuits, where shape selection during growth generate functionalities critical to life, e.g. coiling of plant tendrils [1], formation of flowers [2] and leaves [3], opening of seedpods [4], pine cones [5] and embryonic development/gastrulation [6]. Synergizing morphogenetic finesse with chemical, physiological signaling is exploited for driving actuation – e.g. closing of Venus flytrap [7] and motility (e.g. amoeboid movement of cells [8] and turning of uni-flagellated bacteria [9]). Stimuli responsive, active materials that transduce a non-mechanical cue into programmable mechanical response have been explored in a range of material systems (e.g. metals, ceramics and polymers [10]) and across length-scales (nano - macro) [11-13]. Triggers include physical stimuli such as temperature, electric field, magnetic field, light, pressure, sound and chemical stimuli such as pH, ionic strength and solvent composition [14, 15]. Traditionally, form flows from microstructure. Embedding anisotropic responsiveness via patterning of the macro/micro/molecular structure enables the emergence of engineered 3D structures such as helices [16], foldable templates [17], topographically manipulated surfaces [18] and biomimetic motifs [19].

In related approaches, light responsive polymers that were exposed to spatiotemporally patterned illumination presented persistaltic motility [20] and programmable shape change [21]. Applying graded illumination during 3D printing

has been used to embed mechanical gradients during the fabrication [22]. In planar films gradients in crosslink density have been harnessed to drive assembly of structures that are prone to undergo non-linear actuation, when exposed to stimuli [23]. Patterning the concentration of gold nanorods in matrix has offered an additional pathway to modulate photothermally driven shape selection [24]. These approaches remain highly complementary to advances in 3D printing of responsive polymers composed of a molecularly ordered matrix. These include extrusion-based patterning approaches [25], magnetically assisted stereolithography [26] and those utilizing the synergy of surface alignment and two-photon polymerization [27].

Here, we exploit confinement to drive mechanical non-linearities that hardcode morphogenetic pathways and actuation modes, while eschewing spatially resolved material programming or training. The idea is to free shape selection from a one-to-one correspondence to the material level blueprinting/training. Instead, we upconvert simpler sample-wide responses into symmetry breaking pathways of shape-selection and dynamic responses. Time-dependent responses are also emergent: ranging from motility derived from an unmodulated stimulus, to articulated jointed mechanisms that self-assemble and manipulate without requiring explicit direction. This work utilizes through-thickness twist of the molecular director in liquid crystalline polymers (LCP) as the primary structural motif (twisted nematic – TN). This director profile remains translationally invariant in the monolithic strips, where the thickness (t: μ m-scale) is much smaller than width and length (w, t0: mm-scale). When unconfined, hitherto flat TN LCP transform into coiled structures, when

heated [16]. Judicious confinement transforms the TN LCP into supercoils, prismatic folded trusses, twisted and bent tape spring geometries. Coaxing structural complexity in this manner allows it to complement and to be contrasted against efforts aimed at utilizing high-resolution patterning [28, 29] and incorporation of topological defects [18] to drive assembly and actuation. These pathways are demonstrated in glassy LCP, where modest levels of strain (\sim 1%) are generated. This enables the generalization of this idea across length-scales by harnessing an array of stimuli-responsive elements, including shape memory alloys, dielectric actuators or even piezoelectrically powered composites. Large strain shape adaptivity is not a necessary ingredient.

2. Experimental Methods

2.1. Materials. Elvamide 8023R (Dupont) was dissolved in methanol with a concentration of 0.12 wt%, and then filtered by 0.2 μ m PTFE membrane syringe filter (Pall). Glass slides (Corning) were cleaned with 2-propanol and then treated with atmospheric air plasma by using the plasma cleaner PDC-32G (Harrick Plasma) for $10 \sim 20$ mins. The Elvamide solution was spin-coated on the glass slides at 2000 rpm for 30 seconds. The surface of 8023R on glass slides were rubbed 30 to 40 times by using a velvet rubbing cloth. The cell was assembled using two glass slides prepared as above that are glued using an epoxy adhesive mixed with 15 μ m spacers. To create the twisted nematic orientation, the cell was assembled with the rubbing direction of the two glass slides orthogonal to each other. The anchoring conditions is defined by the rubbing direction. Subsequent introduction of a mesogenic mixture creates a

twisted nematic orientation with the chiral dopant biasing the handedness of the twist. We used RMM34C (Merck) as the mesogenic monomer, Irgacure 784® (bis(cyclopentadienyl)bis[2, 6-difluoro-3-(1-pyrryl)phenyl]titanium (Ciba) as the photo-initiator, and R1011 (Merck) as the right-handed chiral dopant. These three compounds were mixed with the ratio of 97:2:1 using a high-speed mixer (Fisher Scientific) and heated to $100\,^{\circ}$ C to form a uniform viscous solution. The solution was infiltrated into the cell by using capillary injection method. The filled cell was gradually cooled 5 °C for each step, and two pieces of polarizer were used to check if the nematic state is achieved. The nematic state appears around $50-55\,^{\circ}$ C. At nematic state the cell is cured using green light of intensity $50\,^{\circ}$ mW/cm² delivered from two high power illuminators MI-150 (Edmund) for 4 hours. The cell was flipped over after 2 hours of curing to make sure both sides are equally cured.

2.2. Fabrication. After curing, the cell is opened, and the twisted nematic liquid crystal polymer film is cut and removed from the glass slide by using sharp blades. The characteristic twisted nematic orientation was verified using polarized optical microscopy (POM). The POM images are shown in the Supplementary Information (Figure SI 1). Strips of suitable dimensions were excised using blades and glued to external constraints or end-to-end using commercially available acrylate glues. A droplet of the glue was dispensed using a needle and the samples were connected and cured.

2.3. Thermomechanical Characterization. Heating was performed either directly on a hotplate (Fisher Isotemp) or in a silicone oil (McMaster) bath. Unlike heating in silicone oil, hotplate heating allows for ultrafast actuations to happen. In both cases, heating rate was 5K/minute. The samples were heated up to 450K, starting from the ambient. The samples were observed using a Mighty Scope Digital Microscope (7 frames/s). High speed characterizations were performed using a PHANTOM V2511 camera.

3. Results and Discussion

3.1. Confinement Up-Converts Shape Complexity. TN films possessing right-handed, through-thickness variation of the nematic director orientation entails a chiral strain generation. The principal contractile strain direction in a material element is determined by the local director orientation. Strips excised from such a film coil, when heated as a result of progressive disruption of the order. Figure 1a illustrates the characteristic behavior of unconstrained TN strips in response to homogeneous heating in a silicone oil bath [16, 30]. The samples are flat at ambient temperature following fabrication. A planar circular centerline is observed for samples with offset $\theta = 0^{\circ}$, where the curvature increases with increasing temperature. However, for $\theta > 0^{\circ}$, shape with a helical centerline possessing a finite torsion is observed. Spiral geometries result. Figures 1b and c illustrate two characteristic parameters of a helical shape, curvature (κ) and torsion (τ), as a function of temperature and θ . The two parameters are calculated by measuring the coil's radius (r) and pitch ($2\pi p$) using $\kappa = r/(r^2 + p^2)$ and $\tau = p/(r^2 + p^2)$. Here,

pitch is defined as the distance for one complete turn in the helix, measured along its axis. *r* and *p* evolve as a function of temperature. The characteristic curvature is of the order of \sim mm⁻¹, which suggests a thermomechanical strain of $\kappa t/_2 \sim 1\%$ for the t=15 µm film that is fabricated from densely crosslinked glassy LCP. The difference between the scaling of stretching energy ($\sim t$) vs bending ($\sim t^3$) involves a switch over in behaviors when $w \gg \sqrt{tR}$ [4]. w is the width of the strip, t is the thickness of the film, and R is the radius of a closed loop created by gluing two ends of strip together, as shown in Figure 1d. This corresponds to $w \sim 100 \, \mu \text{m}$, which is exceeded in the samples considered here and ensures the preponderance of bending modes during structural evolution. Rigidly confining the ends of the TN strip with $\theta = 0^{\circ}$ modifies the shape selection upon heating (Figure 1a; bottom panel). Since, the longitudinal actuation (along the long axis) is suppressed due to the rigid constraint, the only available actuation mode is contraction along the short axis. Essentially, the Face 2 of the strip on the underside drives the thermomechanical response by generating contractile strains perpendicular to the long axis of the sample. Transverse curvature emerges with a radius of curvature $r \sim 0.8$ mm, corresponding to a strain of $\sim 0.9\%$ (ϕ in the inset $\sim 120^{\circ}$).

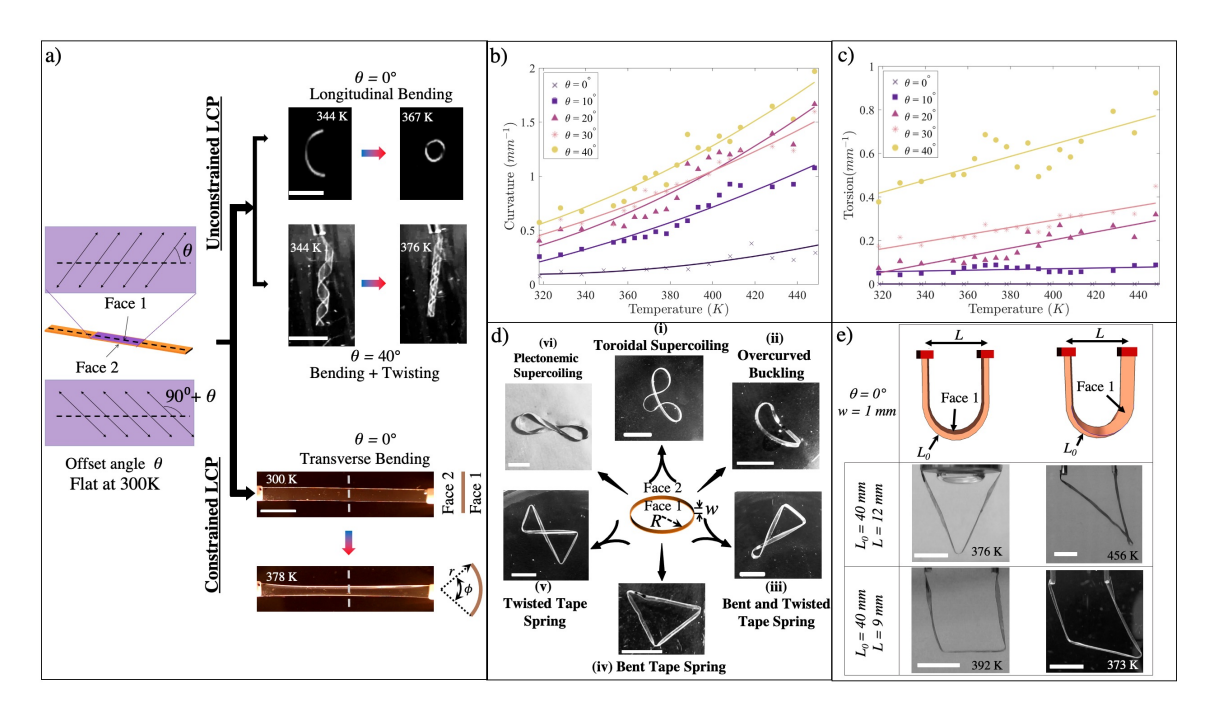


Figure 1: Thermomechanical response of LCP is encoded by its intrinsic molecular ordering and the confinement to which it is subjected. a) Unconstrained TN LCP twist and/or bend as a function of the offset angle θ of the molecular director with respect to the long axis of the flat strips. Constraining the ends of the LCP strip suppresses the strains along its long axis. The ability to generate strains transverse to the long axis (along w: width along short axis) remains, which leads to the creation of a transverse curved sample. $r \sim 0.8$ mm and $\phi \sim 120^{\circ}$. b) Curvature (κ) of the unconstrained strips is a function of temperature; curvature increases with the thermomechanical strain. c) The magnitude of the torsion (τ) in the unconstrained strips also increases with temperature. $\theta = 0^{\circ}$ samples only bend and do not generate twist at any temperature. d) Topological confinement (fixed linking number) of the twisted nematic LCP by connecting them end-to-end elicits an array of structural evolutions, including (i) toroidal supercoiling (θ : 20° , R: 6mm, w: 0.5

mm, T: 392K), (ii) overcurved buckling (θ : θ °, R: 4mm, w: θ .5 mm, T: 347K), strain localization in (iii) bent and twisted tape spring (θ : θ °, R: 6mm, w: 1 mm, T: 335K), (iv) bent tape spring (θ : θ °, R: 4mm, w: 1 mm, T: 433K), and (v) twisted tape spring (θ : θ °, R: 4mm, w: 1 mm, T: 409K) configurations, as well as (vi) plectonemic supercoiling (θ : θ °, T: 340K, R: 6mm, w: 1 mm). e) Confinement of strips in rectangular elasticas where the LCP are rigidly fixtured with their ends facing each other is used to generate spontaneously folded structures. Inducing a twist to one of the faces by $\pi/2$ breaks the left-right symmetry of the structure upon thermal actuation. All scale bars are 5mm.

Figure 1d illustrates rings crafted from TN samples, where they are connected end-to-end. These samples are topologically confined to a fixed linking number. The idea was to explore the shape selection that is emergent from the mechanical frustration between the shape the strips wish to achieve vs. that dictated by the fact they are linked end-to-end. This is roughly motivated by the observation of supercoiling observed in DNA plasmids [31]. Indeed, we observe the plectonemic supercoiling, where the ring becomes an '8' shape for θ = 40° at T=340 K (R = 6 mm, w = 1 mm). Note that this transformation occurs with the linking number fixed at zero, implying that the twist + writhe that is generated during the transformation remains conserved to zero [32]. This supercoiling is distinct from rods where twist is pre-imposed in rods before it connected end-to-end, from which supercoiled response is elicited to mimic DNA plasmids [33, 34]. For samples of smaller width (w = 0.5 mm) and offset (θ = 20°), toroidal supercoiling is observed [35]. Such coiling has been

observed and studied in the contexts of "elastic sewing machine" [36], organized growth of nanotubes [37], supercoiling of DNA plasmids with intrinsic bends [38, 39] and twisted/bent elastic rings [31, 40]. In θ = 0° samples with R = 4 mm and w = 0.5 mm, thermomechanical actuation induces out-of-plane writhe of the centerline. The unconfined θ = 0° sample bends to develop curvature. However, it cannot adopt its natural curvature, when confined in a ring. As a result, it behaves as an "overcurved" ring whose centerline is described by Salkowski curves [41]. This behavior is also analogous to that observed in bi-layered LCP rings that were 3D printed and stimulated with heat [26].

The confined TN LCP in Figure 1a illustrates the role of transverse curvature, which provides additional pathways for shape selection. $\theta=0^\circ$ samples with w=1 mm are found to generate a transverse curvature for R=4 mm. The slender 15 μ m thick geometry prefers to bend rather than stretch and emulates tape-springs that are subjected to bending [42, 43]. The samples localize the bending and concentrate the Gaussian curvature. The ring generates 3 folded joints to transform into a triangle. Beginning with a developable geometry (ring), folding and strain focusing is spontaneous without requiring any localized microstructural patterning or a spatially concentrated stimulus. Utilizing a moderate offset angle of $\theta=10^\circ$ is found to generate sufficient twist to drive the transformation into a bow-tie structure (twisted tape spring) in Figure 1d. On the other hand, increasing R to 6 mm with $\theta=0^\circ$ and W = 1mm reduces the mechanical frustration and the strain localization to create a coat hanger shaped structure (twisted and bent tape spring). Such strain focusing holds

implications for origami-based assembly ideas, but without requiring explicit programming of the folds [44]. Thus, the structural complexity of TN LCP is upconverted by their confinement in rings, beyond their nascent ability to create spiral geometries.

This behavior is also observed in rectangular elasticas that are bent and rigidly fixtured with their faces parallel to their ends as illustrated in Figure 1e (left panel). Here, the responses are parameterized as a function of the distance between the points of fixturing (L) and the length of the prior flat samples (L_o). Samples with w=1 mm and $\theta=0^o$ with $L_o=40$ mm were explored. For L=12 mm, the samples are found to create single fold truss, while for L=9 mm, the greater mechanical frustration from the larger prior curvatures nucleates two folds. We explored the effect of inducing a clockwise $\pi/2$ twist to the strip before fixturing as illustrated in Figure 1e (right panel). The pre-biased twist breaks the left-right symmetry of the structures that are created following heating. The interplay of boundary conditions and prebiased curvature, twist enables new pathways for self-assembling structures by breaking the explicit link between microstructure and shape selection. Broad families of structures are generated.

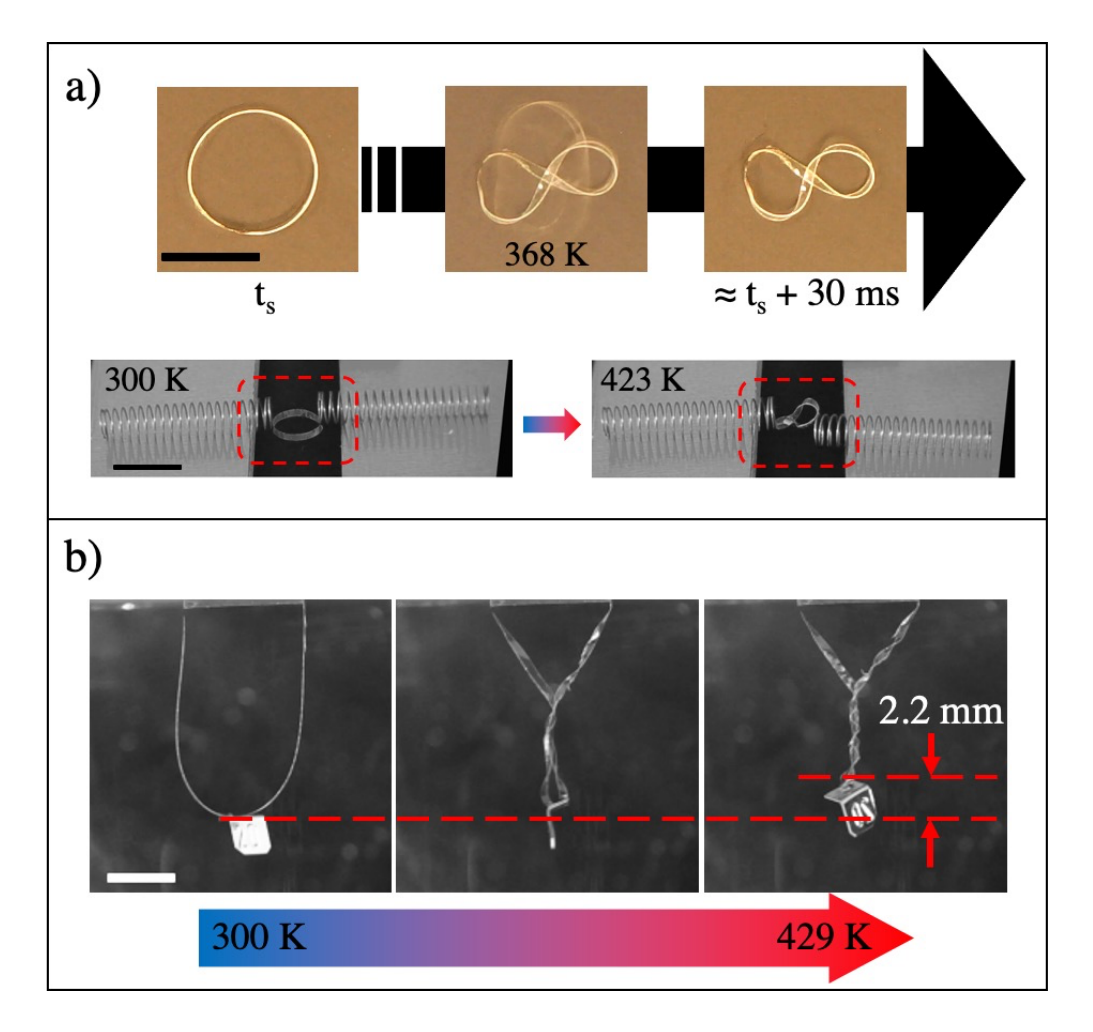


Figure 2: Plectonemic supercoiling generates mechanical work. a) The transformation of a ring with R=4 mm, w=0.5 mm and $\theta=20^{\circ}$ occurs at a mstime scale following heating. The sample builds up strain energy until it reaches the edge of the plectonemic instability. Then, snap-through occurs and the ring is converted into an 8-shape. This is harnessed to move a spring that is 182 mg in weight using the LCP actuator that is 0.74 mg in weight. b) Plectonemic supercoiling in rectangular elasticas is used to lift a 20 mg weight, as the sample is progressively heated. $L_0=40$ mm, L=12 mm, w=1 mm and $\theta=40^{\circ}$. All scale bars are 5 mm.

3.2. Power and Work-Density of the Actuation. The power and work density of the shape transformations are characterized from the time-sequenced images of the actuation. R = 4 mm ring fabricated with w = 0.5 mm and $\theta = 20^{\circ}$ was placed on a hotplate (Figure 2a). The temperature was gradually increased, while the sample was imaged (See SI Movie 1). The sample is found to transition to the 8-shape to commence the plectonemic supercoiling via an ultrafast instability at T=368 K. This is similar to the Zajac instability [45], with the distinction that the linking number remains an invariant in our ring. Thus, twist + writhe = 0 and the generation of the writhe is compensated for by two twists of -1/2 magnitude on both sides. The actuation during this transformation was found to proceed at the ms-time scales as revealed by the high-speed imaging (See SI Movie 2). To harness the work from such actuation, two metallic springs (each weighing 182 mg; McMaster) were glued at two diametrically opposite points of the LCP ring (weighing 0.74 mg) and the system was placed on a hotplate (See SI Movie 3). As the sample is heated, it undergoes a fast transition to the 8-shape and overturns one of the springs by imparting a torsional impulse. To characterize the work content, high speed image sequences of the actuation were analyzed. Image sequences shown in the Supplementary Information (Figure SI2) illustrate how the transition to the 8-shape occurs in 117ms, which displaces the spring by ~7mm. An average velocity of ~0.06m/s is imposed on the 182mg spring. The total kinetic energy (E_k) that results is $E_k = \frac{1}{2}mv^2 + \frac{1}{2}I\omega^2$. Assuming rolling without slip, $v = r\omega$ and the moment of inertia $I \sim mr^2$, $E_k \sim mv^2$. The total energy, weight specific work, power and specific work delivered were computed to be 0.7 μ J, ~0.9 J/kg, 5.6 μ W and 1.2 kJ/m³ respectively. The density of LCP is taken as ~1400 kg/m³.

The plectonemic supercoiling was explored in rectangular elasticas (Figure 2b). A progressively tightly coiled plectoneme emerges with increasing temperatures. The resulting supercoiled shape has the potential to be a useful actuator, as revealed by analogous twisted yarn systems [46]. Here, a 20 mg load was hung from the rectangular elastica, which corresponds to an LCP to load weight ratio of 1:26. The total length of the LCP was 40 mm (L_0) and the distance between the fixturing points (L) was set to 12 mm (also see Figure 1d). Heating the θ = 40° sample (w = 1 mm) induces snarling [47] and decreases its height. The suspended mass is raised against gravity. The total and volume specific work were computed to be 0.45 μ J and 1.1 kJ/m³, respectively. The actuation sequence is also shown in SI Movie 4.

3.3. Phase Space of Shape Selection. The fundamental mode of elastic instability of a twisted ring is transformation to the 8-shape and the higher order modes consist of hierarchically coiled rings which can be categorized under various families depending on the number of terminal loops e.g. β -family (three terminal loops/semiloops) and γ -family (four terminal loops/semi-loops), following the categorization of Coleman and Swigon [31]. The transformation of the ring to the 8 and its progressive twisting onto itself corresponds to the α -family. A time-temperature-series tracking of the structural evolution of the ring shaped elasticas revealed an array of supercoiled geometries. A unified description of the shape diversity that accounts for

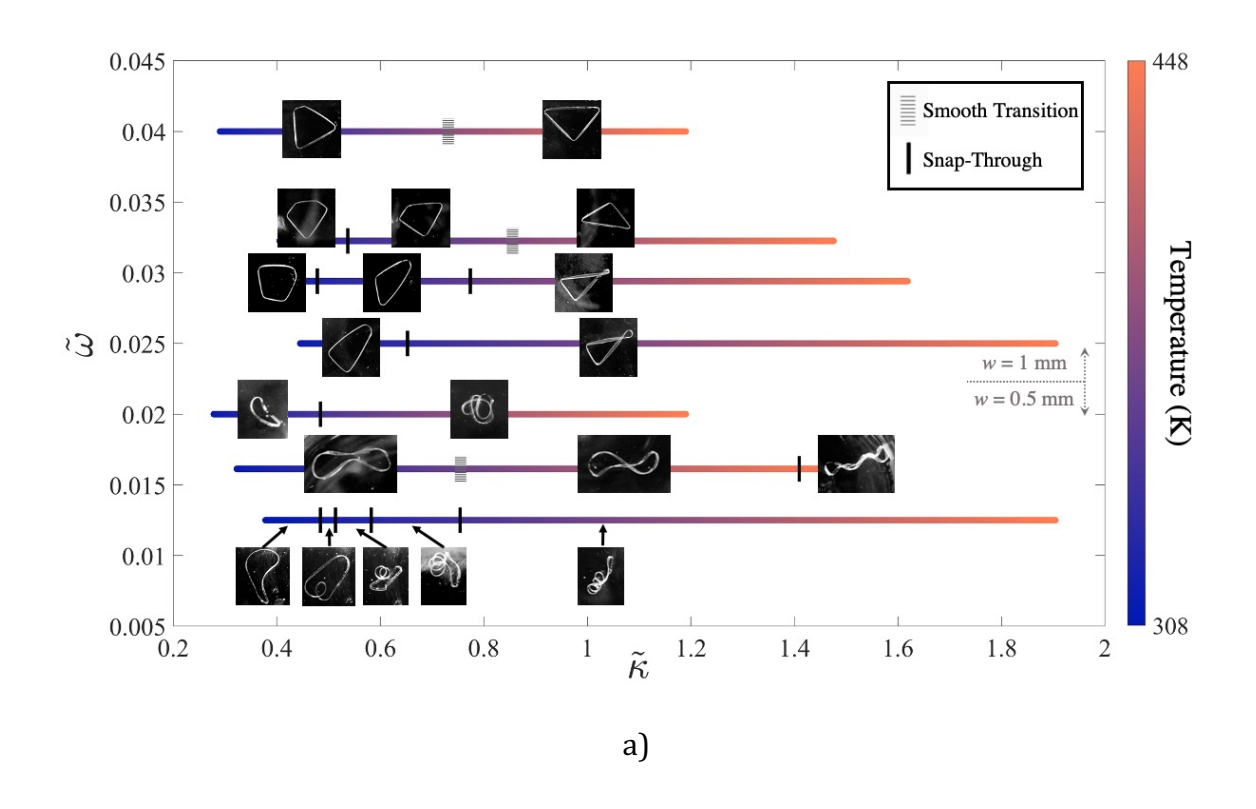
the mechanical non-linearity of TN LCP strips in the presence of self-contact is currently beyond our reach. In Figure 3, we present the array of geometries on a phase space that is parameterized as a function of the geometry. Two variables that define the nascent response of the TN LCP films are the curvature and torsion (Figures 1b and 1c). Samples with $\theta = 0^{\circ}$ only bend and do not produce twist. For these samples, the phase space is parametrized using their normalized curvature, $\tilde{\kappa} = R\kappa$. Here, R is the radius of the ring and κ is the natural curvature that the TN LCP would adopt if it were unconfined at a given temperature (Figure 1b). This normalized curvature is analogous to the overcurvature factor in Ref. [41]. Larger the overcurvature, the greater is the out-of-plane buckling.

The dimensions of the ring were varied by fabricating them from TN LCP strips of lengths ranging from 2.5 to 4 cm. The width of the strip w was varied from 0.5 to 1mm. The width was normalized with respect to the length: $\tilde{\omega} = {}^w/_{2\pi R}$. As seen in Figure 3a, ribbons with a larger width create a transverse curvature to emulate the mechanics of tape springs [42]. Prismatic shapes with strain focused corners emerge. Narrower ribbons, however, deform by twisting and generating loops. The structural evolution is characterized by snap-through transitions that are ultrafast at certain temperatures. These transition points are highlighted in the phase diagram. However, past these transitions, the structural evolution is gradual between the shapes (smooth transition). The effect of offset angle (θ) on the structural evolution of ribbons is shown in Figure 3b. Here, the geometric dimensions including radius of the ring $(R = 6.5 \ mm)$, width of the ribbon $(w = 0.5 \ mm)$, and thickness of the film $(t = 15 \ mm)$

 μm) are kept constant. In this case, $\tilde{\kappa}=R\kappa$ and $\tilde{\tau}=L_0\tau$ are used to parameterize the phase space where $\tilde{\kappa}$ is the overcurvature factor defined previously. τ is the twist the TN LCP would adopt if it were unconfined at a given temperature (Figure 1c); $L_0=2\pi R$. Unlike the ribbons of $\theta=0^\circ$ a finite offset angle generates spiral geometries. $\tilde{\tau}$ is a product of the natural torsion of the ribbons and their total length. As shown in Figure 3b, by increasing the offset angle of the ribbons the effect of torsion becomes more dominant. For $\theta \leq 30^\circ$ trefoil-like structures that fall under the β -family category are observed [31]. At lower temperatures (e.g. $\theta=30^\circ$ at $\sim 350 \text{K}$) toroidal supercoiling is observed. This is a feature observed in DNA plasmids when dye molecules are introduced among base pairs [35]. For larger angles (e.g., $\theta=30^\circ$) the ribbons form structures closer to α -family, that is characterized by plectonemic supercoiling. Thus, the TN LCP, as a function of the offset angle and geometry is found to subsume an array of mechanics ranging from tape spring instabilities to the various classes of supercoiling phenomena observed in DNA plasmids, when $\theta > 0^\circ$.

3.4. Spontaneous Motility and Manipulation. Figure 4a illustrates a supercoiled structure that self assembles from a ring that is placed on a hotplate. The mechanics of shape selection leads to a structure with a broken left-right symmetry, with a distinctive head and tail region. This transformation is spontaneous, when the sample is gradually heated from the ambient to 443K. Upon reaching this temperature, the sample seeks to continue to supercoil (See SI Movie 5). However, the mechanical constraint provided by the hot plate prevents the sample from turning over and continue to supercoil – the strains continue to build in the sample. The strain energy

from the tail that seeks progressive twisting deforms the head, which encounters friction from the surface. When, the threshold for static friction is breached, the sample advances. This mechanism of actuation is essentially perpetual and continues without either spatial or temporal modulation of the heat source and without any texturing of the surface itself. A constant thermal stimulus powers a motile structure with motion that is directed along its axis.



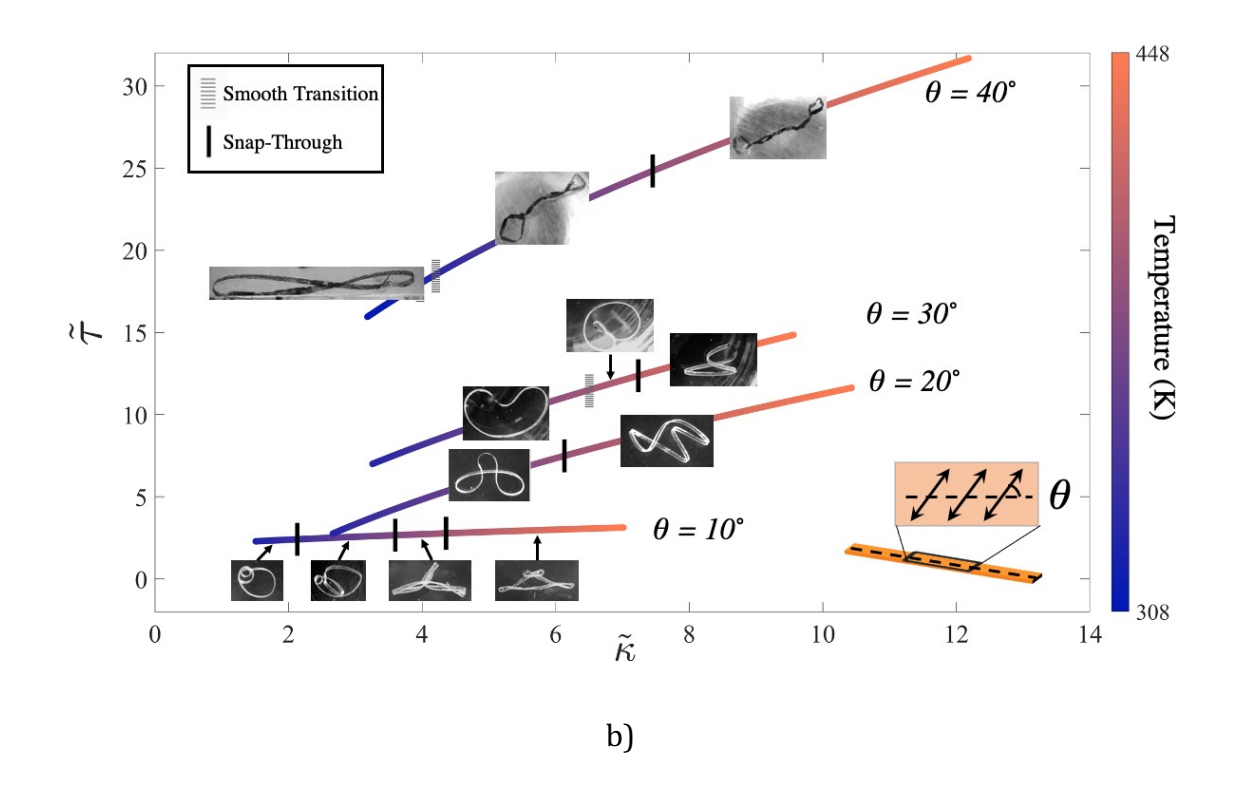


Figure 3: Structural diversity emerging from topologically confined TN LCP rings as a function of geometry and temperature. a) Behavior of θ = 0° TN LCP rings as a function of geometry. $\tilde{\kappa}=R\kappa$. R is the radius of the ring and κ is the natural curvature that the TN LCP would adopt if it were unconfined. The width was normalized with respect to the length: $\tilde{\omega}={}^W/_{2\pi R}$. b) Behavior of θ > 0° TN LCP rings with R=6.5 mm, W=0.5 mm and t=15 μ m. $\tilde{\tau}=L_0\tau$, where τ is the twist the TN LCP would adopt if it were unconfined at a given temperature. $L_0=2\pi R$.

Figure 4b illustrates a rectangular elastica, where one of the ends is twisted clockwise by $\pi/2$ before being fixtured. As shown in Figure 1e, this leads to the assembly of a folded tape spring structure. Continued actuation of this structure

revealed a pathway for self-assembled kinematic mechanisms (SI Movie 6). Figure 4b illustrates the transformation of the rectangular elastica into a bent tape spring configuration. Each bend can be thought of as a joint and a linkage spans the joints. When the sample is progressively heated, the linkage marked iii continues to rotate counterclockwise. This is found to rotate the link marked i counterclockwise as well. However, at a temperature in the vicinity of 433K, the continued rotation of link iii exceeds a threshold angle and the link i rotates clockwise. This is the characteristic crank-rocker kinematic mechanism. Here, we find that this mechanism spontaneously assembles and is driven by simply heating the confined LCP. Manipulation becomes possible without selective powering of individual linkages and joints, which is fundamentally different from how traditional designs of kinematic mechanisms are designed.

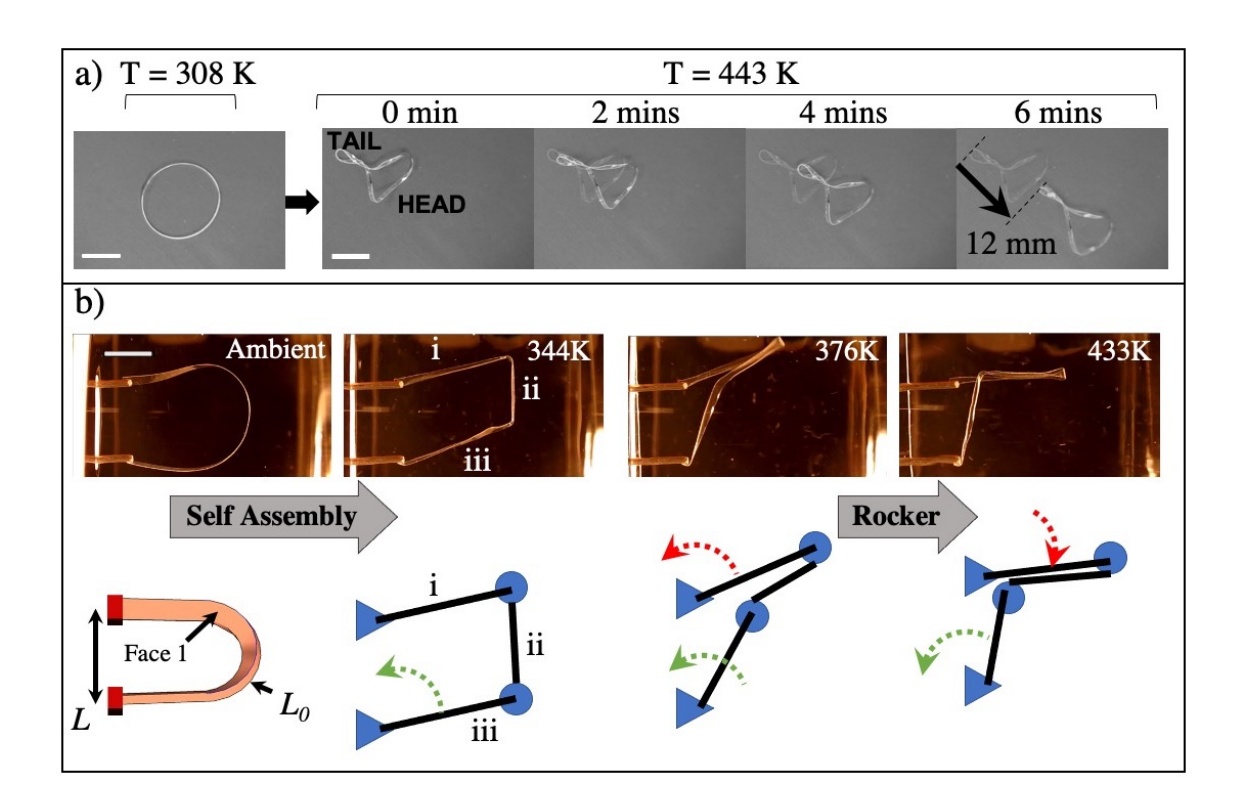


Figure 4: a) A supercoiled geometry that can spontaneously traverse on a hotplate. A distinctive head and tail form. The interplay between the structural evolution and the constraint provided by the surface against progressive coiling of the structure leads to a build-up of the strains. Releasing these strains in bursts to overcome the friction of the surface drives the motility without requiring modulation of the actinic heat source, either in time or in space. R = 6mm, w = 0.5 mm and $\theta = 20^{\circ}$. The starting position is overlaid in translucent rendering to illustrate the displacement of the sample. b) Rectangular elastica that is prebiased with a clockwise $\pi/2$ twist undergoes progressive actuation in silicone oil. Increasing temperature leads to a skewed geometry, which emulates the essential features of a crank-rocker mechanism. The linkage iii rotates in a counterclockwise direction with increasing temperature. However, this triggers a back-and-forth rocking motion in the link i. The ability to selfassemble and emulate kinematic mechanisms in confined LCP emerges. L_0 = 40 mm, L = 9 mm, w = 1 mm and $\theta = 0^{\circ}$. All scale bars are 5 mm.

3.5. Fixity and Hierarchical Assemblies. The thermomechanical responses of LCP are reversible. However, the self-contacting in supercoiled structures is a framework for tuning the mutual mechanical locking and the persistence of the geometries. When the hotplates are switched off and the samples are cooled down to room temperature in the same silicone oil bath (cooling rate: 5° K/min), different levels of fixity are observed. Figure 5 shows three examples with a) negligible, b) partial and c) complete recovery to the initial shapes. Figure 5a illustrates a rectangular elastica fabricated

from a θ = 30° strip (L/L_o = 12 mm/30 mm), which undergoes plectonemic supercoiling that remains locked-in. A twist-tie self-assembles and remains fixed once the thermal stimulus is removed. Figure 5b and c illustrate rings fabricated from θ = 20° with R = 5 mm and R = 4 mm, respectively. We find that Figure 5c, which demonstrates hierarchical toroidal supercoiling with negligible self-contact and interlocking, the recovery to the prior shape is complete. On the other hand, Figure 5b features plectonemic supercoiling with extensive self-contact, which partially precludes the recovery to the initial shape. Thus, a framework emerges for dialing-in the level of shape fixity by modulating the pathways of shape selection.

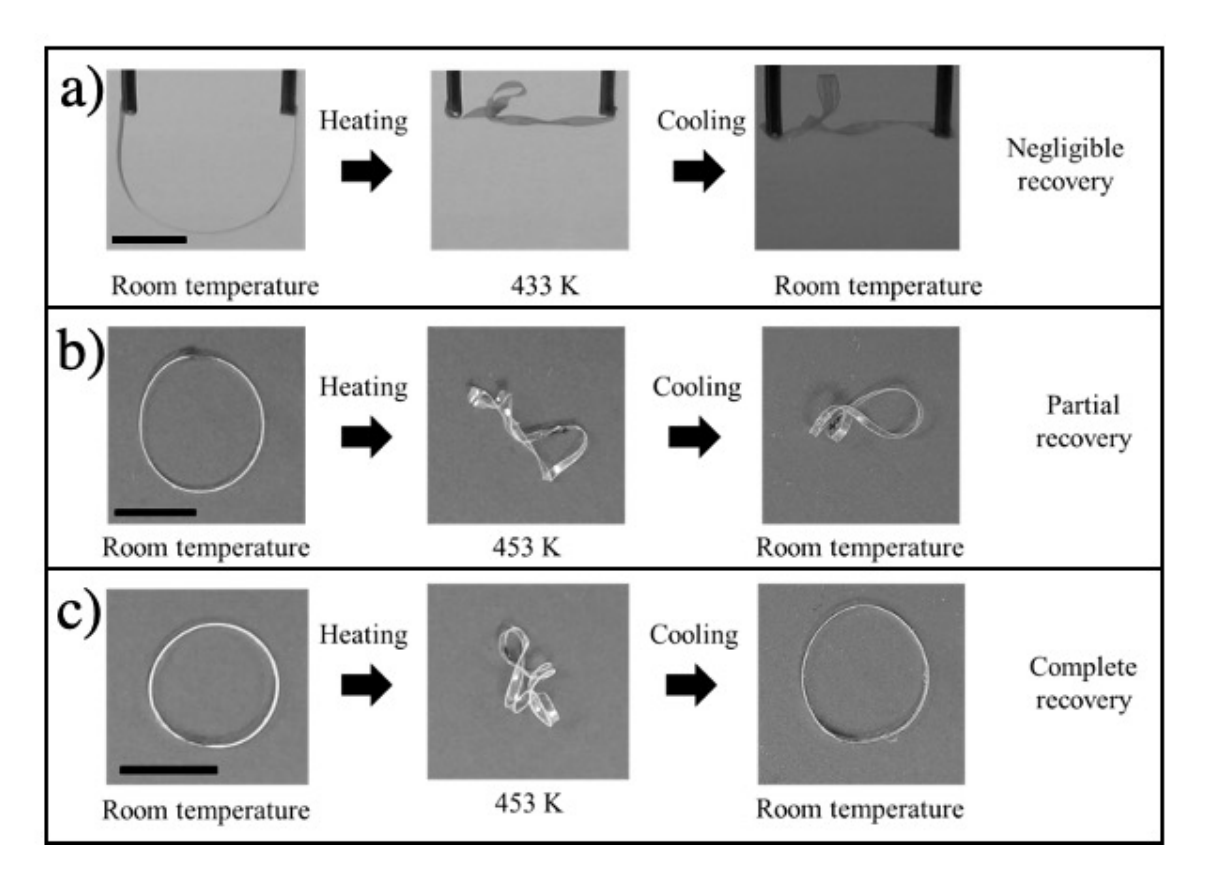


Figure 5: Shape fixity is a function of the level of self-contact. a) Negligible recovery occurs following a heating-cooling cycle, where the sample extensively supercoils

upon itself. b) Moderate recovery occurs in plectonemically self-contacted rings. c)

Toroidal supercoiling is characterized by negligible self-contact, which does not stand
in the way of the recovery upon cooling. All scale bars are 5 mm.

Given the palette of morphogenetic pathways, it is possible to envision superstructures composed from these elements. Figure 6 presents a snapshot of some possibilities. We find that with interconnected rings, they respond individually, but also interact with each other to create assembled structures. Figure 6a illustrates the assembly of hand/arm configuration from w = 0.5 mm rings, while a triplet of $\theta = 0^{\circ}$ rings create an airframe-like structure in Figure 6b (w = 1 mm). Figure 6c illustrates a ring that is partially segmented into two parts via a cut along the length and at the middle of its width. Their mutual interaction and the intrinsic mechanics under confinement is shown to generate structures that mimic a hairpin for w = 2 mm or a jointed supercoiled structure for w = 1 mm depending on the offset angle θ of the parent ring.

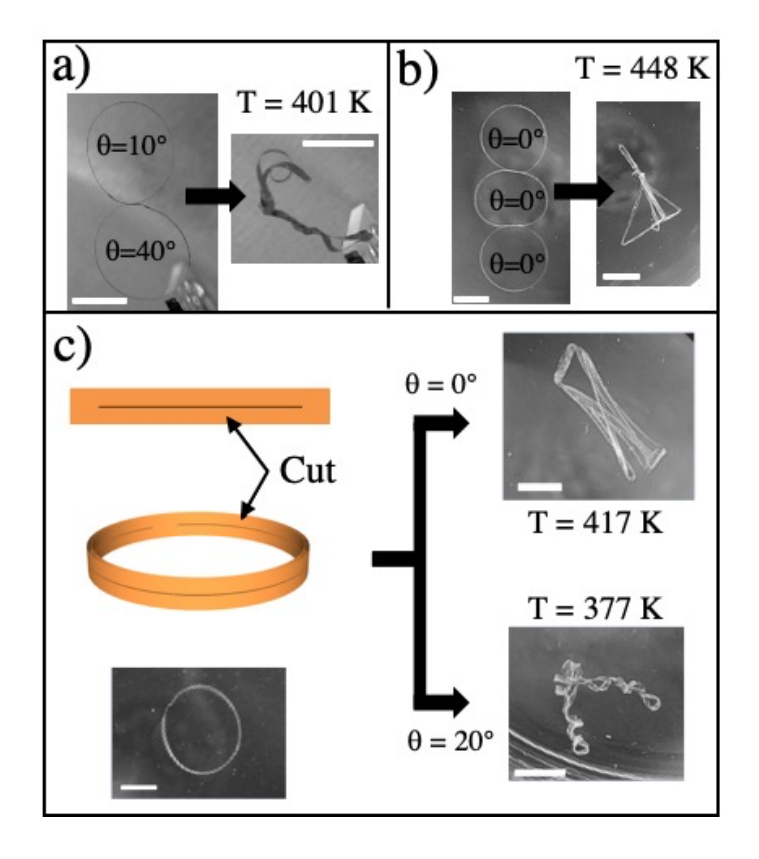


Figure 6: Assemblages of the responsive LCP rings enable superstructures. a) Controlling the offset angles in two rings that are attached to each other elicits overcurved buckling in one (hand) and plectonemic supercoiling in the other (arm). b) A triplet of rings creates an airframe like structure upon thermal stimulation. c) Segmenting a ring via a cut that only runs partially across the sample creates symmetric structures that are a function of θ . All scale bars are 5mm.

4. Conclusions. Complex structures can emerge by harnessing simple nascent responses under judiciously designed confinement. Here, liquid crystalline polymers with a twisted nematic pattern are used. Strips excised from such materials curl, when subjected to a thermal stimulus. However, confining these twisted nematic

strips in rings and rectangular elasticas triggers a hierarchical structural evolution. The one-to-one link between microstructure and form in blueprinted active matter is broken. Instead, we observe supercoiling (toroidal and plectonemic), overcurved buckled rings, bent tape spring with the attendant strain focusing and twisted tape spring configurations. The progressive structural evolution during such self-assembly offer opportunities for impulsive actuation. Supercoiled structures also manifest directional motility by harnessing a constant heat source. The ability to self-assemble tape spring-mimicking structures is used to create kinematic mechanisms that manipulate in a crank-rocker type modality. This time varying response profile is emergent and results from an unstructured thermal stimulus applied to confined twisted nematic polymers. These responses present a pathway towards hierarchical superstructures composed from the confined polymers and are shown to enable tunable shape fixity, airframe-like geometries and hand-arm mimicking structures with functional applications.

Acknowledgement

Support from the National Science Foundation (1635966 and 1921842) is acknowledged. We are also thankful to the reviewers, whose suggestions helped develop a significantly improved manuscript.

References:

- 1. Gerbode, S.J., J.R. Puzey, A.G. McCormick, and L. Mahadevan, How the cucumber tendril coils and overwinds. Science, 2012. **337**(6098): p. 1087-1091.
- 2. Liang, H. and L. Mahadevan, Growth, geometry, and mechanics of a blooming lily. Proceedings of the National Academy of Sciences, 2011. **108**(14): p. 5516-5521.
- 3. Sharon, E., B. Roman, and H.L. Swinney, Geometrically driven wrinkling observed in free plastic sheets and leaves. Physical Review E, 2007. **75**(4): p. 046211.
- 4. Armon, S., E. Efrati, R. Kupferman, and E. Sharon, Geometry and mechanics in the opening of chiral seed pods. Science, 2011. **333**(6050): p. 1726-1730.
- 5. Reyssat, E. and L. Mahadevan, Hygromorphs: from pine cones to biomimetic bilayers. Journal of The Royal Society Interface, 2009. **6**(39): p. 951-957.
- 6. Keller, R., L.A. Davidson, and D.R. Shook, How we are shaped: The biomechanics of gastrulation. Differentiation, 2003. **71**(3): p. 171-205.
- 7. Forterre, Y., J.M. Skotheim, J. Dumais, and L. Mahadevan, How the Venus flytrap snaps. Nature, 2005. **433**(7024): p. 421-425.
- 8. Norberg, B., U. Bandmann, and L. Rydgren, Amoeboid movement in human leucocytes: basic mechanisms, cytobiological and clinical significance. Journal of Mechanochemistry & Cell Motility, 1977. **4**(1): p. 37-53.
- 9. Son, K., J.S. Guasto, and R. Stocker, Bacteria can exploit a flagellar buckling instability to change direction. Nature Physics, 2013. **9**(8): p. 494-498.

- 10. Huang, W.M., Z. Ding, C.C. Wang, J. Wei, Y. Zhao, and H. Purnawali, Shape memory materials. Materials Today, 2010. **13**(7–8): p. 54-61.
- 11. Zhang, J., X. Ke, G. Gou, J. Seidel, B. Xiang, P. Yu, W.-I. Liang, A.M. Minor, Y.-H. Chu, G. Van Tendeloo, X. Ren, and R. Ramesh, A nanoscale shape memory oxide.

 Nature Communications, 2013. **4**(1): p. 1-8.
- 12. Shankar, M.R., M.L. Smith, V.P. Tondiglia, K.M. Lee, M.E. McConney, D.H. Wang, L.S. Tan, and T.J. White, Contactless, photoinitiated snap-through in azobenzene-functionalized polymers. Proceedings of the National Academy of Sciences, 2013. **110**(47): p. 18792-7.
- 13. Rita, J., E.P. Jamie, M.E. Maragakis, D. Reginald, and M.S. Saiidi, Large scale testing of nitinol shape memory alloy devices for retrofitting of bridges. Smart Materials and Structures, 2008. **17**(3): p. 035018.
- 14. Berg, G.J., M.K. McBride, C. Wang, and C.N. Bowman, New directions in the chemistry of shape memory polymers. Polymer, 2014. **55**(23): p. 5849-5872.
- 15. Liu, Y., J. Genzer, and M.D. Dickey, "2D or not 2D": Shape-programming polymer sheets. Progress in Polymer Science, 2016. **52**: p. 79-106.
- 16. Lee, K.M., T.J. Bunning, and T.J. White, Autonomous, Hands-Free Shape Memory in Glassy, Liquid Crystalline Polymer Networks. Advanced Materials, 2012. **24**(21): p. 2839-2843.
- 17. Mao, Y., K. Yu, M.S. Isakov, J. Wu, M.L. Dunn, and H. Jerry Qi, Sequential Self-Folding Structures by 3D Printed Digital Shape Memory Polymers. Scientific Reports, 2015. **5**: p. 13616.

- 18. McConney, M.E., A. Martinez, V.P. Tondiglia, K.M. Lee, D. Langley, I.I. Smalyukh, and T.J. White, Topography from Topology: Photoinduced Surface Features Generated in Liquid Crystal Polymer Networks. Advanced Materials, 2013. **25**(41): p. 5880-5885.
- 19. Gladman, S.A., E.A. Matsumoto, R.G. Nuzzo, L. Mahadevan, and J.A. Lewis, Biomimetic 4D printing. Nature Materials, 2016. **15**(4): p. 413-418.
- 20. Palagi, S., A.G. Mark, S.Y. Reigh, K. Melde, T. Qiu, H. Zeng, C. Parmeggiani, D. Martella, A. Sanchez-Castillo, and N. Kapernaum, Structured light enables biomimetic swimming and versatile locomotion of photoresponsive soft microrobots. Nature Materials, 2016. **15**(6): p. 647-653.
- 21. Hauser, A.W., D. Liu, K.C. Bryson, R.C. Hayward, and D.J. Broer, Reconfiguring nanocomposite liquid crystal polymer films with visible light.

 Macromolecules, 2016. 49(5): p. 1575-1581.
- 22. Kuang, X., J. Wu, K. Chen, Z. Zhao, Z. Ding, F. Hu, D. Fang, and H.J. Qi, Grayscale digital light processing 3D printing for highly functionally graded materials. Science Advances, 2019. **5**(5): p. eaav5790.
- 23. Lee, D.-W., J. Phadikar, and M.R. Shankar, Multiplicity of shape selection in functionally graded liquid crystalline polymers. RSC Advances, 2017. **7**(37): p. 23046-23054.
- 24. Kuenstler, A.S., Y. Chen, P. Bui, H. Kim, A. DeSimone, L. Jin, and R.C. Hayward,
 Blueprinting Photothermal Shape Morphing of Liquid Crystal Elastomers.

 Advanced Materials, 2020. **32**(17): p. 2000609.

- 25. Kotikian, A., R.L. Truby, J.W. Boley, T.J. White, and J.A. Lewis, 3D printing of liquid crystal elastomeric actuators with spatially programed nematic order.

 Advanced Materials, 2018. **30**(10): p. 1706164.
- 26. Tabrizi, M., T.H. Ware, and M.R. Shankar, Voxelated molecular patterning in three-dimensional freeforms. ACS Applied Materials & Interfaces, 2019. 11(31): p. 28236-28245.
- 27. Guo, Y., H. Shahsavan, and M. Sitti, 3D Microstructures of Liquid Crystal Networks with Programmed Voxelated Director Fields. Advanced Materials, 2020. **32**(38): p. 2002753.
- 28. Guo, Y., M. Jiang, C. Peng, K. Sun, O. Yaroshchuk, O. Lavrentovich, and Q.H. Wei, High resolution and high throughput plasmonic photopatterning of complex molecular orientations in liquid crystals. Advanced Materials, 2016. **28**(12): p. 2353-2358.
- 29. Ware, T.H., M.E. McConney, J.J. Wie, V.P. Tondiglia, and T.J. White, Voxelated liquid crystal elastomers. Science, 2015. **347**(6225): p. 982-984.
- 30. Sawa, Y., F. Ye, K. Urayama, T. Takigawa, V. Gimenez-Pinto, R.L. Selinger, and J.V. Selinger, Shape selection of twist-nematic-elastomer ribbons. Proceedings of the National Academy of Sciences, 2011. **108**(16): p. 6364-6368.
- 31. Coleman, B.D. and D. Swigon, Theory of Supercoiled Elastic Rings with Self-Contact and Its Application to DNA Plasmids. Journal of Elasticity and the Physical Science of Solids, 2000. **60**(3): p. 173-221.

- 32. Bauer, W.R., R.A. Lund, and J.H. White, Twist and writhe of a DNA loop containing intrinsic bends. Proceedings of the National Academy of Sciences, 1993. **90**(3): p. 833-837.
- 33. Thompson, J.T., G.M. van der Heijden, and S. Neukirch, Supercoiling of DNA plasmids: mechanics of the generalized ply. Proceedings of the Royal Society of London. Series A: Mathematical, Physical and Engineering Sciences, 2002. **458**(2020): p. 959-985.
- 34. Irobalieva, R.N., J.M. Fogg, D.J. Catanese Jr, T. Sutthibutpong, M. Chen, A.K. Barker, S.J. Ludtke, S.A. Harris, M.F. Schmid, W. Chiu, and L. Zechiedrich, Structural diversity of supercoiled DNA. Nature Communications, 2015. **6**(1): p. 1-11.
- 35. Calladine, C., Toroidal elastic supercoiling of DNA. Biopolymers: Original Research on Biomolecules, 1980. **19**(10): p. 1705-1713.
- 36. Jawed, M.K. and P.M. Reis, Pattern morphology in the elastic sewing machine. Extreme Mechanics Letters, 2014. 1: p. 76-82.
- 37. Geblinger, N., A. Ismach, and E. Joselevich, Self-organized nanotube serpentines. Nature Nanotechnology, 2008. **3**(4): p. 195-200.
- 38. Laundon, C.H. and J.D. Griffith, Curved helix segments can uniquely orient the topology of supertwisted DNA. Cell, 1988. **52**(4): p. 545-549.
- 39. Yang, Y., T.P. Westcott, S.C. Pedersen, I. Tobias, and W.K. Olson, Effects of localized bending on DNA supercoiling. Trends in Biochemical Sciences, 1995.20(8): p. 313-319.

- 40. Griffith, B.E. and S. Lim, Simulating an elastic ring with bend and twist by an adaptive generalized immersed boundary method. Communications in Computational Physics, 2012. **12**(2): p. 433-461.
- 41. Mouthuy, P.-O., M. Coulombier, T. Pardoen, J.-P. Raskin, and A.M. Jonas, Overcurvature describes the buckling and folding of rings from curved origami to foldable tents. Nature Communications, 2012. **3**: p. 1290.
- 42. Seffen, K. and S. Pellegrino, Deployment dynamics of tape springs. Proceedings of the Royal Society of London. Series A: Mathematical, Physical and Engineering Sciences, 1999. **455**(1983): p. 1003-1048.
- 43. Soykasap, Ö., Analysis of tape spring hinges. International Journal of Mechanical Sciences, 2007. **49**(7): p. 853-860.
- 44. Liu, Y., J.K. Boyles, J. Genzer, and M.D. Dickey, Self-folding of polymer sheets using local light absorption. Soft Matter, 2012. **8**(6): p. 1764-1769.
- 45. Zajac, E., Stability of two planar loop elasticas. Journal of Applied Mechanics, 1962. **29**(1): p. 136-142.
- 46. Haines, C.S., M.D. Lima, N. Li, G.M. Spinks, J. Foroughi, J.D. Madden, S.H. Kim, S. Fang, M.J. De Andrade, and F. Göktepe, Artificial muscles from fishing line and sewing thread. Science, 2014. **343**(6173): p. 868-872.
- 47. Goss, V.G.A., G.H.M. Heijden, J.M.T. Thompson, and S. Neukirch, Experiments on snap buckling, hysteresis and loop formation in twisted rods. Experimental Mechanics, 2005. **45**(2): p. 101-111.